Transition to Chronic Fibrosis in an Animal Model of Retinal Detachment With Features of Proliferative Vitreoretinopathy

Cornelia Peterson,[1,2] Yuchen Lu,[3] Clayton P. Santiago,[4] Antoinette C. Price,[3] Minda M. McNally,[3] William Schubert,[5] Khaled Nassar,[5] Thomas Zollner,[5] Seth Blackshaw,[4] Charles G. Eberhart,[3,6] and Mandeep S. Singh[3,7]

[1]Department of Molecular and Comparative Pathobiology, Johns Hopkins University School of Medicine, Baltimore, Maryland, United States
[2]Department of Comparative Pathobiology, Tufts University, Cummings School of Veterinary Medicine, North Grafton, Massachusetts, United States
[3]Wilmer Eye Institute, Johns Hopkins University School of Medicine, Baltimore, Maryland, United States
[4]Solomon H. Snyder Department of Neuroscience, Johns Hopkins University School of Medicine, Baltimore, Maryland, United States
[5]Bayer AG, Wuppertal, Germany
[6]Department of Pathology, Johns Hopkins University School of Medicine, Baltimore, Maryland, United States
[7]Department of Genetic Medicine, Johns Hopkins University School of Medicine, Baltimore, Maryland, United States

Correspondence: Mandeep S. Singh, Wilmer Eye Institute, Johns Hopkins Hospital, 600 N. Wolfe St, Baltimore, MD 21287, USA; mandeep@jhmi.edu.
Charles G. Eberhart, Wilmer Eye Institute, Johns Hopkins Hospital, 600 N. Wolfe St, Baltimore, MD 21287, USA; ceberha@jhmi.edu.

Received: January 9, 2023
Accepted: September 18, 2023
Published: December 28, 2023

Citation: Peterson C, Lu Y, Santiago CP, et al. Transition to chronic fibrosis in an animal model of retinal detachment with features of proliferative vitreoretinopathy. *Invest Ophthalmol Vis Sci.* 2023;64(15):39. https://doi.org/10.1167/iovs.64.15.39

Purpose. Proliferative vitreoretinopathy (PVR) is the most common cause of failure of surgically repaired rhegmatogenous retinal detachment (RRD). Chemically induced and cell injection PVR models do not fully simulate the clinical characteristics of PVR in the post-RRD context. There is an unmet need for translational models in which to study mechanisms and treatments specific to RRD-PVR.

Methods. RRD was induced in adult Dutch Belted rabbits. Posterior segments were fixed or processed for RNA sequencing at 6 hours and 2, 7, 14, and 35 days after induction. Histochemical staining and immunolabeling for glial fibrillary acidic protein, alpha smooth muscle actin, vascular endothelial growth factor receptor 2, CD68, and RPE 65 kDa protein were performed, and labeling intensity was scored. Single cell RNA sequencing was performed.

Results. Acute histopathological changes included intravitreal and intraretinal hemorrhage, leukocytic vitritis, chorioretinitis, and retinal rarefaction. Chronic lesions showed retinal atrophy, gliosis, fibrotic subretinal membranes, and epiretinal fibrovascular proliferation. Fibrillar collagen was present in the fibrocellular and fibrovascular membranes in chronic lesions. Moderate to strong labeling of glia and vasculature was detected in chronic lesions. At day 14, most cells profiled by single cell sequencing were identified as Müller glia and microglia, consistent with immunolabeling. Expression of several fibrillar collagen genes was upregulated in chronic lesions.

Conclusions. Histological and transcriptional features of this rabbit model simulate important features of human RRD–PVR, including the transition to chronic intraretinal and periretinal fibrosis. This animal model of RRD with features of PVR will enable further research on targeted treatment interventions.

Keywords: epithelial–mesenchymal transition, epiretinal membrane, tractional retinal detachment, vitrectomy, gliosis, fibrosis, collagen, GFAP, αSMA, RPE65, VEGFR2, CD68

Proliferative vitreoretinopathy (PVR), characterized by retinal contraction and periretinal proliferation, is the most common cause of failure after rhegmatogenous retinal detachment (RRD) repair.[1–6] There is currently no effective pharmacological treatment or prophylaxis agent available for this postoperative complication, and the cellular components and molecular drivers of PVR are incompletely elucidated. However, inflammation, the release of cytokines, altered expression of growth and transcription factors, and induction of epithelial-to-mesenchymal transition (EMT) of RPE cells, fibroblasts, and glia have all been suggested as key factors.[7–20] Proposed targets for intervention include ligands, agonists, and inhibitors of cytokine and growth factor signaling pathways, but there remains an unmet need for effective PVR therapies and appropriate animal models of disease in which to evaluate them.[12,18,21–29]

The pathogenesis of RRD–PVR has historically been characterized by five developmental stages. The stages are disruption of the blood–retinal barrier, resulting hypoxia, leukocyte chemotaxis and migration to the site of injury,

EMT, and proliferation of epiretinal, intraretinal, and subretinal cells, critically, involving a substantial role of activated Müller glial cells in the remodeling of the extracellular matrix (ECM) with membrane production and fibrotic contraction.[2–4,6,17,18,25,30–34] However, the proportion and distribution of specific cell types involved, and temporal and spatial regulation of these processes, are poorly understood. The objective of the current study was to more comprehensively identify pertinent cell populations and describe the histological progression in a refined rabbit model of RRD. Here we present the cell types and ECM features of disease progression in RRD with features of PVR and demonstrate acute changes (primarily inflammation and hemorrhage) through the transition to epiretinal fibrovascular and subretinal fibrocellular membranes and chronic gliosis.

Methods

Model Induction

This study was approved by the Johns Hopkins University's Institutional Animal Care and Use Committee (protocol number: RB20M263). All animal experiments were performed in accordance with the guidelines for the Use of Animals in Ophthalmic and Vision Research of ARVO and in adherence with the ARRIVE 2.0 Guidelines.[35] Adult female Dutch Belted rabbits (1.5–2.5 kg) obtained from Robinson Services Inc (Mocksville, NC, USA) were maintained in a temperature-controlled, 12-hour light cycle environments with ad libitum food and water. Briefly, animals were anesthetized with ketamine (35 mg/kg intramuscularly) and xylazine (5 mg/kg intramuscularly), intubated, and maintained on isoflurane. A refined approach to unilateral induction of RRD with feature of PVR was achieved via lensectomy, pars plana vitrectomy, large retinotomy, and iatrogenic retinal detachment induction by subretinal injection of saline, followed by retinal cryotherapy and intravitreal autologous platelet-rich plasma injection ($n = 3$ rabbits/time point); contralateral globes, receiving only enrofloxacin (5 mg/kg subconjunctivally once postoperatively), lidocaine (1 mg/kg subconjunctivally once postoperatively), and dexamethasone SP (0. 5mg/kg subconjunctivally once postoperatively), served as controls.[36]

In Vivo Grading

In vivo retinal assessments were performed using indirect ophthalmoscopy at 6 hours and 2, 7, 14,, and 35 days after RRD induction and scored using standardized PVR scoring schemes as shown in Supplementary Table S1.[37–39]

Histology and Immunocytochemistry

Animals were humanely euthanized 6 hours and 2, 7, 14, and 35 days after RRD induction. Posterior segments of enucleated globes were harvested and then either fixed in 10% neutral-buffered formalin or 4% paraformaldehyde in PBS or stored at −80°C for later processing. Routine hematoxylin and eosin staining of 5-µm-thick formalin-fixed, paraffin-embedded and paraformaldehyde-fixed, OCT-embedded sections were used to evaluate full-thickness retinal morphology and morphology of the inner retina with associated fibrovascular membranes, respectively. Masson's trichrome staining, performed on all formalin-fixed, paraffin-embedded sections by the JHMI Reference Histology Laboratory, was used to localize collagen expression. Immunohistochemical staining for RPE 65 kDa protein (RPE65) was performed on all formalin-fixed, paraffin-embedded sections, and immunofluorescent staining for glial fibrillary acidic protein (GFAP), alpha smooth muscle actin (αSMA), vascular endothelial growth factor receptor 2 (VEGFR2), and CD68 was performed on all frozen sections using standard protocols and details as presented in Supplementary Table S2. Tissue sections were evaluated using an Olympus BX50 (Tokyo, Japan) and an Olympus AX70, respectively. The percentage of cells with positive labeling was estimated, and labeling intensity was evaluated to generate a semiquantitative staining score (0, absent; 1, weak, focal; 2, moderate, multifocal; and 3, strong, diffuse) independently by two pathologists (CP, CGE).

RNA Sequencing

Extracted retinas ($n = 2$ per time point) were dissociated into single cells and processed to evaluate transcription profiling using single cell RNA-Seq (10X Genomics, Pleasanton, CA, USA); UMAP analysis was performed to profile cell populations at day 14 after induction and compared with controls, as described elsewhere.[40] For heatmap analysis, collagen expression z-scores were obtained from log-transformed and pseudobulked transcript counts in control retina and lesions harvested at days 14 and 35, respectively. All rabbit sequencing data can be accessed at GEO accession numbers GSE217333. Code used to analyze the data sets in this study can be found at https://github.com/csanti88/pvr_singlecell_vs_singlenucleiRNAseq_2022.

Statistical Analyses

The median PVR grade was determined using Prism 8 GraphPad (v. 9.2.0; San Diego, CA, USA) and recorded over time. Correlation of median PVR grades with collagen staining was analyzed by Fisher's exact test and two-tailed t tests. The mode of semiquantitative immunolabeling scores was determined and recorded over time. The single cell RNA sequencing (scRNA-seq) data were analyzed using R statistical language (R Core Team v. 4.1.0; Vienna, Austria). Default parameters in Seurat's FindMarkers function was used to find differentially expressed genes using a non-parametric Wilcoxon rank sum test, and adjusted P values were obtained from Bonferroni corrections applied to all genes in the dataset ($\alpha = 0.05$).

Results

In Vivo Grading

The median grades of PVR severity for all classification schemes used increased over time with the exception of day 14 after induction, when scored using the Blumenkranz model, as shown in the Table.

No classification schemes were significantly correlated with collagen deposition.

Distinct Histopathological Features of Acute, Subacute, and Chronic Lesions

We classified histopathological changes as acute (6 hours to 2 days), subacute (7 days), and chronic (14 days and beyond) based on classical histological features of

Investigative Ophthalmology & Visual Science

Table. Median PVR Severity Grades Over Time

Time Point (*n*)	Hida	Blumenkranz	Fastenberg
Control (3)	0	0	1
H6 (2)	5.5	2.5	3.5
D2 (3)	6	3	4
D7 (3)	6	3	4
D14 (2)	6.5	2	4
D35 (3)	7	3	5

immune response and tissue remodeling (acute inflammation, subacute proliferation, chronic remodeling) used broadly at multiple sites in the body.[41] Retinas obtained from control animals demonstrated no significant hemorrhage, necrosis, or inflammation (Figs. 1A, B). Acute histopathological changes (hour 6 and day 2) included intravitreal, intraretinal, and choroidal hemorrhage, and infiltration of the vitreous, retina, choroid, and orbital soft tissues by large numbers of both degenerate and nondegenerate heterophils and fewer numbers of macrophages. Heterophils are leukocytes in rabbits, which are functionally similar to neutrophils in humans.[42–45] Rarefaction, edema, and fibrin deposition of the inner nuclear layers was also observed in the acute phase (Figs. 1C–F). Sections of necrotic foci were present with swollen, hypereosinophilic ganglion cells containing pyknotic nuclei and disruption of photoreceptor outer segments in regions overlying subretinal fibrinosuppurative exudates.

Subacute changes observed on day 7 included full-thickness retinal folds and persistent edema and rarefaction of the inner retina admixed with infiltrating microglia. Vitreal hemorrhage had nearly resolved at this time point; however, a mixed population of inflammatory cells remained in the vitreous and subretinal space, and erythrophagocytosis was observed. Early atrophic change, particularly of the outer retina, and gliosis were also present by day 7 (Figs. 2A, B). Chronic lesions (days 14 and 35) included panretinal atrophy and progressive gliosis, highlighted by prominent radial Müller glia (Supplementary Fig. S1). Subretinal fibrocellular membranes, often with anterior dispersion of single RPE cells through the inner retina, and epiretinal fibrovascular

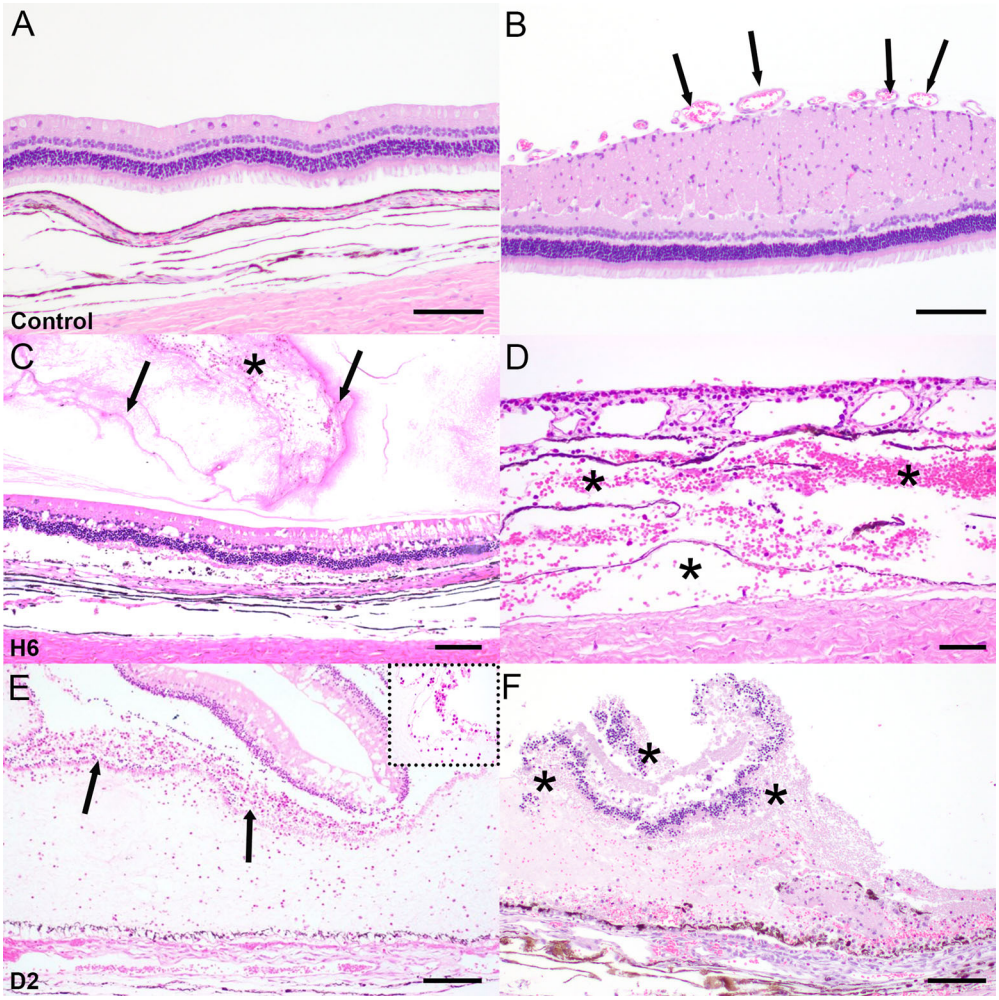

Figure 1. Representative histology of the normal control retina and acute histopathological lesions following unilateral induction of RRD–PVR. No significant hemorrhage, inflammation, or rarefaction were observed within the control neural retina (**A**) or the medullary streak (**B**; *arrows* indicate surface vasculature). Moderate to severe vitreal hemorrhage (*asterisk*) and fibrin exudation (*arrows*) (**C**) and moderate to severe choroidal hemorrhage (*asterisks*) (**D**) were observed at 6 hours after induction. Acute heterophilic inflammation within the subretinal space (*arrows*) (**E**) with inflammatory cells shown at higher magnification (*inset*) and foci of necrosis of the neural retina (*asterices*) (**F**) were observed 2 days after induction. Scale bar, 50 µM.

Investigative Ophthalmology & Visual Science

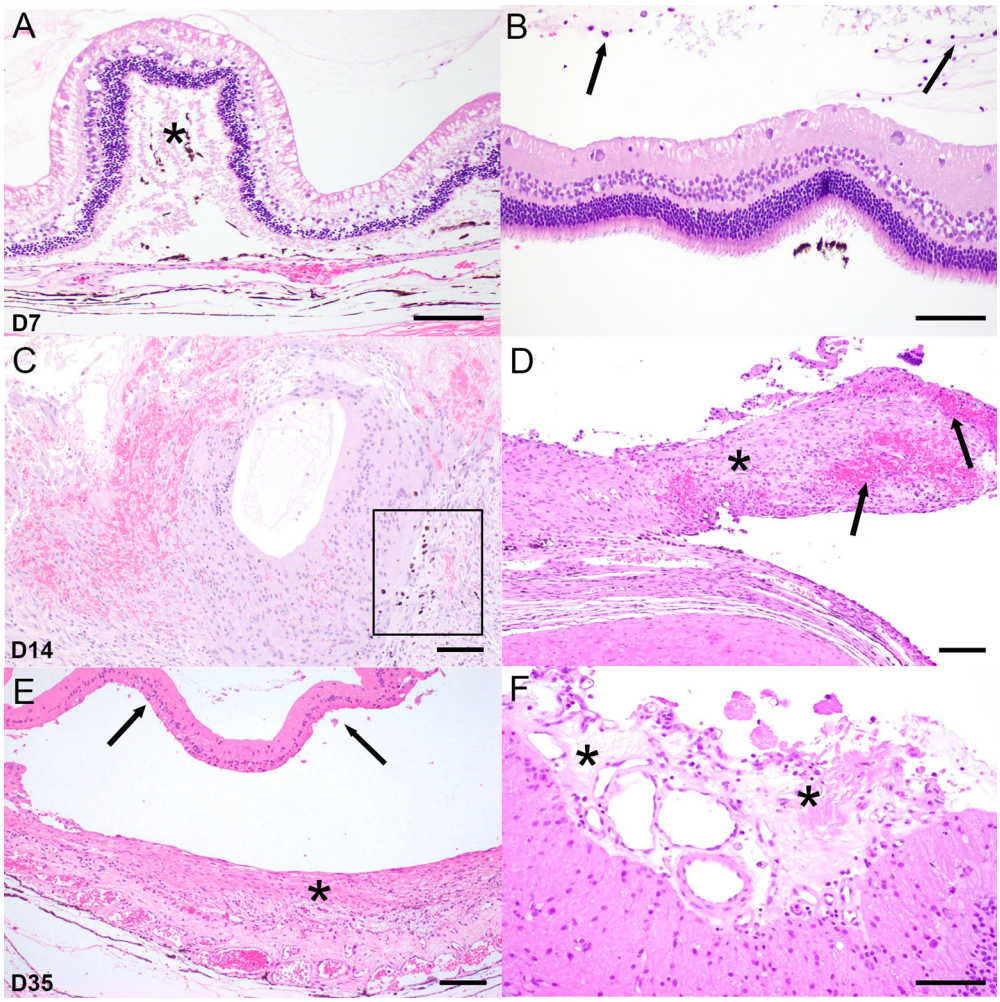

Figure 2. Representative histology of subacute and chronic histopathological lesions after unilateral induction of RRD–PVR. Progressive rarefaction of the inner neural retinal layers along with full-thickness retinal folds (*asterisk*) (**A**) and moderate infiltration of the vitreous by a mixed population of inflammatory cells (*arrows*) (**B**) were present at day 7 after induction. Resolving hemorrhage, moderate to severe atrophy, and full-thickness folding of the neural retina with anterior migration of pigmented RPE cells (*boxed area*) (**C**) and the formation of subretinal fibrocellular membranes (*asterisk*) with intramembranous hemorrhage (*arrows*) (**D**) were observed at day 14 after induction. At day 35 after induction, progressive, dense fibrous subretinal membranes (*asterisk*) were attached to the RPE and Bruch's membrane posterior to the detached and atrophic retina (*arrows*) (**E**). Dense epiretinal fibrovascular membranes (*asterisks*) were also observed in the region of the medullary streak (**F**). Scale bar, 50 µM.

membranes in the region of the medullary streak were also observed at later time points (Figs. 2C–F).

Progressive Accumulation of Fibrillar Collagen in Epiretinal and Subretinal Membranes

To assess the location and extent of epiretrinal and subretinal membranes containing collagenous components, we conducted trichrome staining. Retinas with acute and subacute lesions were trichrome negative; however, trichrome-positive strands of fibrillar collagen were observed within the vitreous at day 2 and day 7. Semiquantitative analysis showed that moderate trichrome positivity began at day 14 and progressed by day 35 (Figs. 3A–G). Chronic lesions exhibited trichrome-positive fibrillar collagen in the subretinal fibrocellular and epiretinal fibrovascular membranes.

We hypothesized that multiple collagen species were involved in periretinal membrane formation. To interrogate gene expression of diverse collagen species, we used scRNA-seq. A heatmap analysis for fibrillar collagen revealed that *COL1A1* was upregulated in Müller glia at day 14 after injury relative to control samples, whereas *COL5A1* and *COL5A2* were upregulated at day 35 after induction relative to controls (Fig. 4A). These data suggest that multiple collagen species may be involved in the formation of pathological PVR membranes in promoting periretinal membrane contractility.

Temporal Expression of VEGFR2 in Fibrovascular Lesions

We observed early epiretinal membrane formation along the posterior face of the vitreous and inner retina in the dorsal and ventral quadrants and more densely organized fibrovascular proliferation in the region of the medullary streak in chronic RRD with features of PVR. To assess the extent and

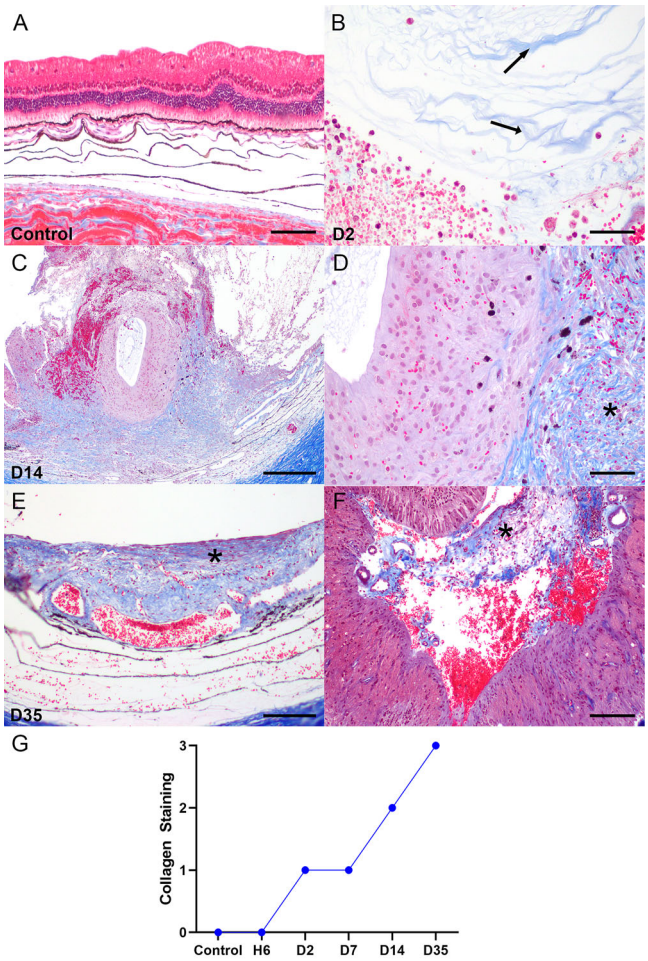

Figure 3. Expression of fibrillar collagen in the rabbit retina following unilateral induction of RRD–PVR. No collagen was observed in the vitreous, retina, or subretinal space in the control tissue (**A**) (Masson's trichrome stain; scale bar, 50 µM). Thin strands of fibrillar collagen (*blue*) were observed in the vitreous in association with acute heterophilic vitritis by day 2 (*arrows*) (**B**) (scale bar, 25 µM). By day 14, the subretinal space was expanded by fibrillar collagen that abutted the folded and gliotic neural retina (**C**) (scale bar, 100 µM). Higher magnification demonstrating intraretinal gliosis and subretinal fibrosis (*asterisk*) (**D**) (scale bar, 50 µM). By day 35, the subretinal membranes (*asterisk*) contained increasing amounts of fibrillar collagen with fewer cellular components (**E**) (scale bar, 100 µM), and the epiretinal fibrovascular membranes of the medullary streak (*asterisk*) comprised a dense collagenous matrix (**F**) (scale bar, 50 µM). The intensity of trichrome staining increased over time (**G**) ($n = 3$ per time point).

temporal pattern by which VEGF signaling may play a role in cell proliferation in the context of these lesions, we stained acute, subacute, and chronic specimens for VEGFR2. In acute and subacute specimens, VEGFR2 was weakly expressed. However, expression of VEGFR2 associated with epiretinal fibrovascular membranes in the medullary streak peaked at day 14 (Figs. 5A–D). There was only moderate expression at day 35.

Microglia and Gliotic Changes

To assess the abundance of microglial cells, we combined CD68 immunolabeling and morphological features, with a small proportion of cells having abundant cytoplasm and a larger eccentric nucleus, a morphology supportive of circulating macrophages; however, the majority of these cells were smaller, with rarefied processes, consistent with microglia. In acute and subacute lesions, CD68 expression, associated with increased numbers of retinal microglia, peaked at days 2 and 7. $CD68^+$ cells were located primarily in the inner retinal layers and epiretinal membranes of the medullary streak (Figs. 5E–H). At chronic time points, $CD68^+$ cells were observed at an intensity and proportion similar to controls. We assayed upregulated expression of GFAP to evaluate Müller glia hypertrophy. $GFAP^+$ Müller glia were restricted to the neural retina (Figs. 6B–E). At day 14 after induction, relatively few neurons were captured by UMAP analysis, and the majority of cells profiled were identified as Müller glia and microglia (Figs. 4B, C).

Subretinal RPE DeDifferentiation and Proliferation

We used RPE65 as a marker of differentiated RPE cells. $RPE65^+$ cells were attenuated (weak to absent) at day 14 relative to controls, with expression loss corresponding to regions of subretinal fibrosis and foci of pigmented cells observed migrating anteriorly through the subretinal membranes toward the interface with the gliotic neural retina (Figs. 7A–D). On day 14, upregulated expression of αSMA within the subretinal fibrocellular membrane indicated dedifferentiation and EMT of RPE cells (Fig. 6C).

Discussion

Both the vasculature and myelinated nerve fibers of the lagomorph retina are confined to the medullary streak, a broad horizontal band ventral to the optic nerve head with a high density of photoreceptors, ganglion cells, and amacrine cells.[46,47] Although the meriangiotic rabbit retina differs from the holangiotic pattern in humans, the distribution of the vessels in the nerve fiber layer are similar to humans, and the number of main arterial branches crossing the disc margin is similar between the two species.[48] As such, despite some differences in vasculature, the rabbit is commonly accepted as an efficient and cost-effective animal model of ophthalmic disease owing to the large globe and inducible proliferation, with dozens of published PVR studies using the rabbit over the past decade.[16,29,49–67]

The epiretinal fibrovascular membranes demonstrated here seem to simulate similar lesions that are commonly found in clinical PVR, and although the subretinal fibrocellular membranes are less commonly encountered in human PVR, they are an important pathological feature, because they alter the capacity for retinal reattachment.[68–70] Existing rabbit models have not consistently demonstrated both epiretinal and subretinal membranes, the key histological features of human PVR.[16,29,52,53,55–57,63,64,67] Our data also demonstrate the involvement of multiple collagen species in the development of collagenous membranes, suggesting that multiple profibrotic signaling pathways may be involved. These rabbit data also validate the presence of additional features of human PVR, that is, increased microglial invasion into epiretinal membranes, Müller glia activation, and RPE dedifferentiation.[71]

Cryotherapy to stimulate local, acute inflammatory responses and the use of PRP to stimulate platelet-secreted

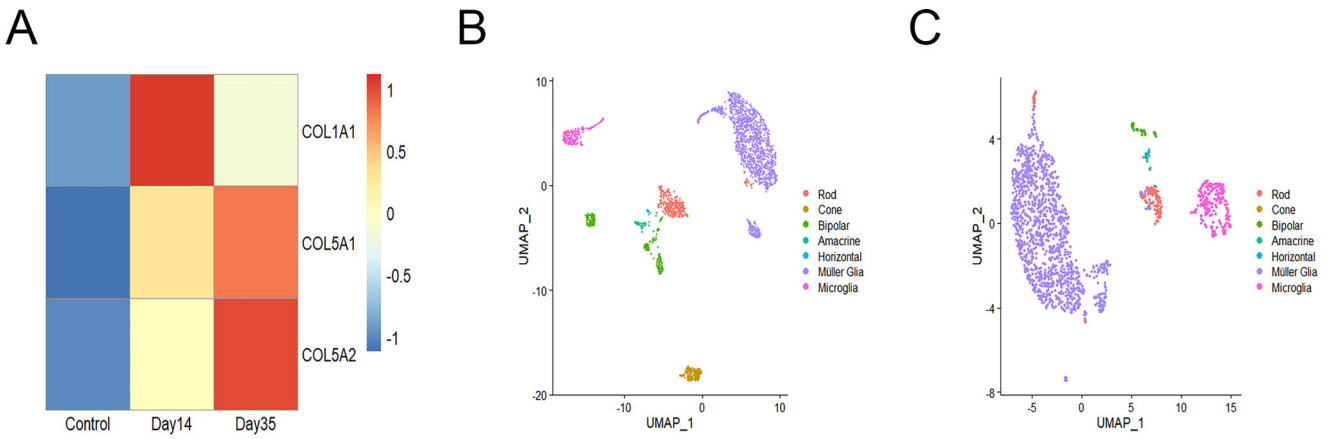

Figure 4. scRNA-seq of the rabbit retina following unilateral induction of RRD-PVR. Heatmap for differentially expressed fibrillar collagen produced by Müller glia demonstrating upregulation in chronic lesions (**A**) ($n = 2$ per time point). UMAP plots for single cell RNA-seq of control rabbit retinas (**B**) and day 14 after unilateral induction of RRD–PVR (**C**). Note the change in the number of cells (Müller glia and microglia) over time.

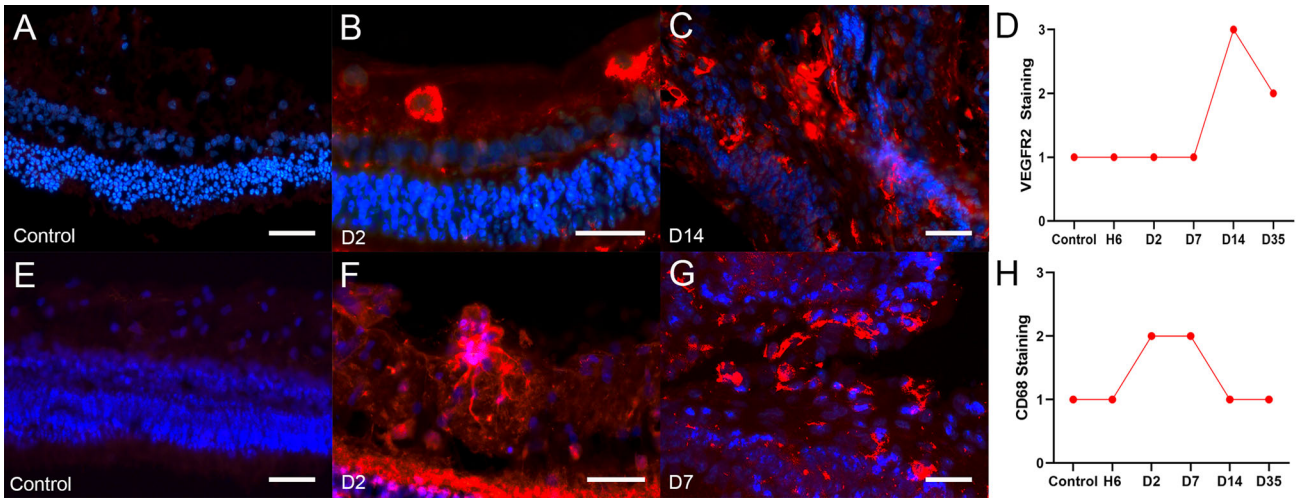

Figure 5. Expression of VEGFR2 and CD68 in the rabbit retina after unilateral induction of RRD–PVR. No labeling of vessels was observed within the neural retina (**A**; *red*, VEGFR2; *blue*, DAPI; scale bar, 25 µM) in the control tissue or at day 2 or day 7 in any region other than the medullary rays (**B**) (scale bar, 10 µM). By day 14, there was a marked increase in the number or small vessels within the inner layers of the medullary streak and in association with epiretinal fibrovascular membranes (**C**) (scale bar, 25 µM). VEGFR2 staining was increased at day 14 and but began to decrease at day 35 (**D**) ($n = 4$ per time point). Weak labeling of microglia was observed within the neural retina in the control tissue (**E**; *red*, CD68; *blue*, DAPI; scale bar, 25 µM). By day 2, there was moderate expression of CD68 by cells morphologically consistent with microglia within the inner layers of the neural retina (**F**) (scale bar, 25 µM). At day 14, there was moderate expression of CD68 by microglia associated with epiretinal fibrovascular membranes in the medullary streak (**G**) (scale bar, 25 µM). CD68 staining peaked at day 2 and day 7 (**H**) ($n = 3$ per time point).

growth factors and cytokines are further advantages of the animal model presented here. We included PRP injection because we, and others, have found that it promotes the development of PVR features in animal models, leading to a more reproducible extent and severity of lesions in our animal cohort. Notably, retinal exposure to blood components in the context of vitreous hemorrhage is recognized as a major risk factor for PVR development in humans. With the majority of human PVR cases developing between 30 and 45 days postoperative, the relatively fast disease progression (subacute to chronic histopathological features by day 7 after induction) represents one discordant feature of our rabbit model.[3,6] The risk of intraoperative hemorrhage with excessive exudation of proinflammatory signals and bias toward subretinal pathology are potential limitations of a surgical model of RRD with features of PVR in the rabbit.[72] The degree of hemorrhage is more than is standard for a routine retinal detachment, and the somewhat traumatic nature of this model is also a limitation.

This manuscript also addresses two main knowledge gaps in the rabbit PVR models, namely, acute changes (6 hours and 2 days) and epiretinal versus subretinal fibrosis. We focused on acute time point analysis because the early pathological changes represent potential treatment targets to prevent more severe retinal damage. Regarding subretinal fibrosis, we feel this key feature has received inadequate attention despite being an important—and surgically chal-

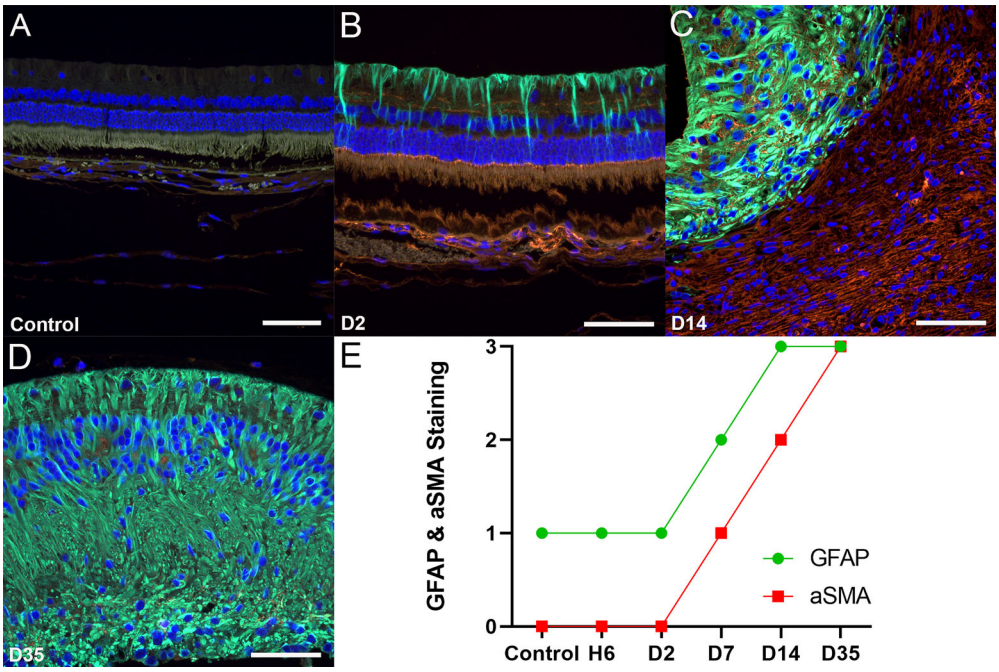

Figure 6. Expression of GFAP and αSMA in the rabbit retina after unilateral induction of RRD–PVR. Weak expression of GFAP by Müller glia within the neural retina was observed in the control globes. αSMA was not expressed in controls (**A**; *red*, αSMA; *green*, GFAP; *blue*, DAPI; scale bar, 50 µM). By day 2, increased GFAP expression by Müller glia was observed within the neural retina (**B**) (scale bar, 50 µM). At day 14, GFAP was strongly expressed by proliferating and hypertrophied Müller glia within the neural retina, and αSMA was strongly expressed within subretinal fibrocellular membranes (**C**) (scale bar, 50 µM). At day 35, gliosis and GFAP expression were diffuse wtihin the neural retina (**D**) (scale bar, 50 µM). The staining of both GFAP and αSMA increased over time (**E**) ($n = 4$ per time point).

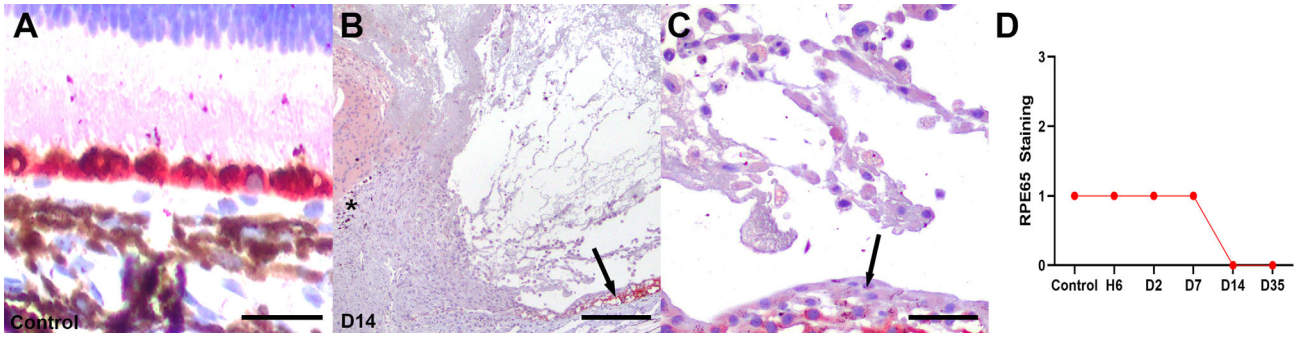

Figure 7. Expression of RPE65 in the rabbit retina following unilateral induction of RRD–PVR. RPE65 expression was observed in the RPE in the control retinas with normal cuboidal architecture (**A**; *red*, RPE65; scale bar, 25 µM). At day 14, RPE65 expression was largely absent in the region of the subretinal membrane (*arrow*) and in foci of migrating pigmented cells (*asterisk*), consistent with dedifferentiation of RPE (**B**) (scale bar, 100 µM). Higher magnification highlighting the loss of RPE65 expression in RPE that have undergone EMT and transitioned from normal cuboidal epithelial cells and assumed a flattened, fibroblastic appearance (*arrow*). Moderate numbers of subretinal heterophils and macrophages are present, several of which contain red bloods cells within the cytoplasm (erythrophagocytosis) (**C**) (scale bar, 25 µM). RPE65 staining decreased over time (**D**) ($n = 4$ per time point).

lenging, in terms of curative intervention—component in the most severe cases of human PVR.[68–70,73,74]

Earlier studies have primarily focused on epiretinal membrane formation. Chen et al.[16] reported disruption of the inner limiting membrane and epiretinal fibrosis in their model after 10 days after lesion induction. In their dataset, critical acute changes occurring earlier than 10 days could not be identified, and data on subretinal membrane formation were not presented.[16] Similarly, histological sections presented in Hirose et al.[63] and Khoroshilova-Maslova et al.[64] demonstrated tractional retinal folds with epiretinal membranes at 4 and 8 weeks after induction. Epiretinal membranes and RPE proliferation were reported at 30 days after induction, but the presence of these histomorphological features was not evaluated at earlier points, and subretinal membranes were also not targeted for analysis.[63,64]

Other investigators report variable degrees of retinal thickening, gliosis, and atrophy.[29] Elevated αSMA expression in epiretinal membranes at time points ranging from 22 days to 11 weeks after induction have been reported, but subretinal data are unavailable.[29,52,53,55,56,67] Khanum et al.[57] reported evaluation of their rabbit model one and 30 days after induction; however, it is unclear from their figures

from which time points their photomicrographs of hematoxylin and eosin–stained or immunolabeled sections were obtained. Our 6-hour and 2-day data broadly align with the findings of Zahn et al.[61] at days 3 and 7 after induction, in which they assayed Müller glia, microglia, and macrophages.

After retinal detachment and disruption of the blood–retinal barrier with subsequent vitreal traction, early immune responses, characterized by leukocyte infiltration of the retina and vitreous and local cytokine and growth factor production, are the nidus for vascularized epiretinal membrane formation in PVR, with mononuclear cells and histiocytes more often implicated in traumatic etiologies.[75–78] In the current study, we demonstrate fibrinohemorrhagic and necrotizing vitritis and chorioretinitis with subsequent heterophilic infiltration by hour 6 and day 2 after induction, respectively. Increasing expression of CD68 within the inner retinal layers of the medullary streak was observed in the subacute period, peaking at days 2 and 7 after induction, with a lag before the development of neovascularization in the fibrovascular epiretinal membranes observed at day 14. Collectively, these results suggest that early damage or ischemia is characterized initially by acute infiltration by heterophils, the subsequent release of proinflammatory cytokines and growth factors, which then, in turn, promote microglial recruitment and neovascularization. Under hypoxic conditions, reduced ubiquitination or TNF-α–mediated induction of hypoxia inducible factor 1α promotes transcriptional activation of hypoxia responsive elements, leading to increased expression of VEGFR2 to restore tissue perfusion.[79,80] The contribution of microglia to the retinal inflammatory response and regulation of retinal and choroidal vasculature has been well-documented, further supporting a role in neovascularization for the microglia observed in association with the fibrovascular epiretinal membranes in the current study.[19,81]

Jin et al.[31] described a key transition in the course of human PVR at day 30 when highly cellular, loosened ECM becomes more densely fibrotic. In the current study, we validate this transition in ECM remodeling of both the epiretinal and subretinal membranes at day 35 after induction with compaction and paucicellularity of the membranes when compared with day 14. Our scRNA-seq data confirm this differential expression of fibrillar collagens over time with upregulation of *COL1A1*, *COL5A1*, and *COL5A2* at days 14 and 35 after induction, respectively. Further, this transition corresponds with an increase in αSMA and fibrillar collagen expression in both the epiretinal and subretinal membranes as demonstrated with immunolabeling and Masson's trichrome staining, respectively. The transition also correlates with increased Müller glia proliferation and hypertrophy as demonstrated by GFAP immunolabeling when compared with controls. GFAP and vimentin are commonly used as markers of retinal gliosis in the context of PVR, and Eastlake et al.[17] reported that numerous inflammatory mediators are expressed by Müller glia in vitro and upregulated in the gliotic retina.[18,82]

In the current study, we demonstrate loss of RPE65 expression by RPE cells by day 14 after induction, corresponding with the same time point that subretinal fibrocellular membrane formation was earliest observed. Additionally, rare, pigmented cells, which were negative for RPE65 labeling and therefore likely to correspond with dedifferentiated RPE cells or possibly choroidal melanocytes, were observed at the anterior margin of these subretinal membranes, abutting the gliotic neural retina. Together, these findings suggest dedifferentiation of RPE cells in response to chronic injury before transforming to a more mesenchymal cell type, and support the notion that the migration of proliferative RPE cells not only contributes to epiretinal membranes, but also subretinal fibrocellular membranes, in PVR.[83]

Failure to adequately sample RPE and subretinal tissue for dissociation and RNA isolation precluded this critical cell population from subsequent sequencing analyses and the opportunity to confirm the dedifferentiation during EMT, observed histologically at day 14 after induction, and represents a limitation of the current study. A further limitation is that the layer-specific distribution (i.e., epiretinal vs. subretinal membrane) of collagen expression is unclear from the current dataset because retinal specimens, including all membranes, were processed together for scRNA-seq.

Conclusions

We demonstrate the cellular and ECM features throughout the time course of lesion development using a rabbit model of RRD with features of PVR. Additionally, using RNA-Seq, we confirm the relevant cell populations present at a critical transition presented at day 14 after induction and identified fibrillar collagen species that are differentially expressed by Müller glia. Development of high-fidelity in vivo models for RRD–PVR are essential for future investigations of targeted treatment interventions.

Acknowledgments

Funded by Bayer AG as part of a sponsored research collaboration with the Wilmer Eye Institute, Johns Hopkins Hospital. Peterson's and Santiago's salary support was provided by NIH T32 OD011089 (PI: Mankowski) and NIH 2T32EY007143 (PI: Zack), respectively.

Meeting Presentation: Partial analyses were presented at the 2022 Association of Research in Vision and Ophthalmology Annual Meeting, Denver, Colorado.

Conflicts of Interest: For this project, MSS received sponsored research support from Bayer as part of a research collaboration of the Wilmer Eye Institute with Bayer. MSS is/was a paid advisor to Bayer Healthcare, Revision Therapeutics, Johnson & Johnson, Third Rock Ventures, Novartis Pharmaceuticals, W. L. Gore & Associates, Deerfield, Trinity Partners, Kala Pharmaceuticals, and Acucela. These arrangements have been reviewed and approved by the Johns Hopkins University in accordance with its conflict-of-interest policies. SB is a co-founder and Scientific Advisory Board member of CDI Labs, LLC, and is/was a paid advisor to Third Rock Ventures and Tenpoint Therapeutics. WS is a paid employee of Bayer Pharma AG. KN is a paid employee of Bayer Pharma AG. TZ is paid employee of Bayer Pharma AG. The remaining authors report no conflicts.

Disclosure: **C. Peterson**, None; **Y. Lu**, None; **C.P. Santiago**, None; **A.C. Price**, None; **M.M. McNally**, None; **W. Schubert**, Bayer Pharma AG (E); **K. Nassar**, Bayer Pharma AG (E); **T. Zollner**, Bayer Pharma AG (E); **S. Blackshaw**, CDI Labs, LLC (O), Third Rock Ventures (C), Tenpoint Therapeutics (C); **C.G. Eberhart**, None; **M.S. Singh**, Bayer (F), Bayer Healthcare (C), Revision Therapeutics (C), Johnson & Johnson (C), Third Rock Ventures (C), Novartis Pharmaceuticals (C), W. L. Gore & Associates (C), Deerfield (C), Trinity Partners (C), Kala Pharmaceuticals (C), Acucela (C)

References

1. Hilton G, Machemer R, Michels R, Okun E, Schepens C, Schwartz A. The classification of retinal detach-

ment with proliferative vitreoretinopathy. *Ophthalmology*. 1983;90(2):121–125.
2. Nagasaki H, Shinagawa K, Mochizuki M. Risk factors for proliferative vitreoretinopathy. *Prog Retin Eye Res*. 1998;17(1):77–98.
3. Pastor JC. Proliferative vitreoretinopathy. *Surv Ophthalmol*. 1998;43(1):3–18.
4. Pastor JC, de la Rúa ER, Martıń F. Proliferative vitreoretinopathy: risk factors and pathobiology. *Prog Retin Eye Res*. 2002;21(1):127–144.
5. Tosi GM, Marigliani D, Romeo N, Toti P. Disease pathways in proliferative vitreoretinopathy: an ongoing challenge. *J Cell Physiol*. 2014;229(11):1577–1583.
6. Idrees S, Sridhar J, Kuriyan AE. Proliferative vitreoretinopathy: a review. *Int Ophthalmol Clin*. 2019;59(1):221–240.
7. Machemer R, van Horn D, Aaberg TM. Pigment epithelial proliferation in human retinal detachment with massive periretinal proliferation. *Am J Ophthalmol*. 1978;85(2):181–191.
8. Yang S, Li H, Li M, Wang F. Mechanisms of epithelial-mesenchymal transition in proliferative vitreoretinopathy. *Discov Med*. 2015;20(110):207–217.
9. Kimura K, Orita T, Fujitsu Y, et al. Inhibition by female sex hormones of collagen gel contraction mediated by retinal pigment epithelial cells. *Invest Ophthalmol Vis Sci*. 2014;55(4):2621–2630.
10. Umazume K, Liu L, Scott PA, et al. Inhibition of PVR with a tyrosine kinase inhibitor, dasatinib, in the swine. *Invest Ophthalmol Vis Sci*. 2013;54(2):1150.
11. Hatanaka H, Koizumi N, Okumura N, et al. Epithelial-mesenchymal transition-like phenotypic changes of retinal pigment epithelium induced by TGF-β Are prevented by PPAR-γ agonists. *Invest Ophthalmol Vis Sci*. 2012;53(11):6955.
12. Cheng HC, Ho TC, Chen SL, Lai HY, Hong KF, Tsao YP. Troglitazone suppresses transforming growth factor beta-mediated fibrogenesis in retinal pigment epithelial cells. *Mol Vis*. 2008;14:95–104.
13. Liang CM, Tai MC, Chang YH, et al. Glucosamine inhibits epithelial-to-mesenchymal transition and migration of retinal pigment epithelium cells in culture and morphologic changes in a mouse model of proliferative vitreoretinopathy. *Acta Ophthalmol (Copenh)*. 2011;89(6):e505–e514.
14. Gamulescu MA, Chen Y, He S, et al. Transforming growth factor beta2-induced myofibroblastic differentiation of human retinal pigment epithelial cells: regulation by extracellular matrix proteins and hepatocyte growth factor. *Exp Eye Res*. 2006;83(1):212–222.
15. Nassar K, Grisanti S, Tura A, et al. A TGF-β receptor 1 inhibitor for prevention of proliferative vitreoretinopathy. *Exp Eye Res*. 2014;123:72–86.
16. Chen XF, Du M, Wang XH, Yan H. Effect of etanercept on post-traumatic proliferative vitreoretinopathy. *Int J Ophthalmol*. 2019;12(5):731–738.
17. Eastlake K, Banerjee PJ, Angbohang A, Charteris DG, Khaw PT, Limb GA. Müller glia as an important source of cytokines and inflammatory factors present in the gliotic retina during proliferative vitreoretinopathy. *Glia*. 2016;64(4):495–506.
18. Wickham L, Charteris DG. Glial cell changes of the human retina in proliferative vitreoretinopathy. *Dev Ophthalmol*. 2009;44:37–45.
19. Fischer AJ, Zelinka C, Milani-Nejad N. Reactive retinal microglia, neuronal survival, and the formation of retinal folds and detachments. *Glia*. 2015;63(2):313–327.
20. Chiba C. The retinal pigment epithelium: an important player of retinal disorders and regeneration. *Spec Issue Stem Cells*. 2014;123:107–114.
21. Lashkari K, Rahimi N, Kazlauskas A. Hepatocyte growth factor receptor in human RPE cells: implications in proliferative vitreoretinopathy. *Invest Ophthalmol Vis Sci*. 1999;40(1):149–156.
22. Kimoto K, Nakatsuka K, Matsuo N, Yoshioka H. p38 MAPK mediates the expression of type I collagen induced by TGF-β2 in human retinal pigment epithelial cells ARPE-19. *Invest Ophthalmol Vis Sci*. 2004;45(7):2431–2437.
23. Kita T, Hata Y, Arita R, et al. Role of TGF-β in proliferative vitreoretinal diseases and ROCK as a therapeutic target. *Proc Natl Acad Sci U S A*. 2008;105(45):17504.
24. Lei H, Kazlauskas A. Growth factors outside of the platelet-derived growth factor (PDGF) family employ reactive oxygen species/Src family kinases to Activate PDGF receptor α and thereby promote proliferation and survival of cells*. *J Biol Chem*. 2009;284(10):6329–6336.
25. Cui J, Lei H, Samad A, et al. PDGF receptors are activated in human epiretinal membranes. *Exp Eye Res*. 2009;88(3):438–444.
26. Rojas J, Fernandez I, Pastor JC, et al. A strong genetic association between the tumor necrosis factor locus and proliferative vitreoretinopathy: the Retina 4 Project. *Ophthalmology*. 2010;117(12):2417–2423.e2.
27. Li H, Wang H, Wang F, Gu Q, Xu X. Snail Involves in the Transforming growth factor β1-mediated epithelial-mesenchymal transition of retinal pigment epithelial cells. *PLoS One*. 2011;6(8):e23322.
28. Chen X, Xiao W, Liu X, et al. Blockade of Jagged/Notch pathway abrogates transforming growth factor β2-induced epithelial-mesenchymal transition in human retinal pigment epithelium cells. *Curr Mol Med*. 2014;14(4):523–534.
29. Ma G, Duan Y, Huang X, et al. Prevention of proliferative vitreoretinopathy by suppression of phosphatidylinositol 5-phosphate 4-kinases. *Invest Ophthalmol Vis Sci*. 2016;57(8):3935.
30. Wilkins RB, Kulwin DR. Wound healing. *Ophthalmology*. 1979;86(4):507–510.
31. Jin Y, Chen H, Xu X, Hu Y, Wang C, Ma Z. Traumatic proliferative vitreoretinopathy: clinical and histopathological observations. *Retina Phila Pa*. 2017;37(7):1236–1245.
32. Sethi CS, Lewis GP, Fisher SK, et al. Glial remodeling and neural plasticity in human retinal detachment with proliferative vitreoretinopathy. *Invest Ophthalmol Vis Sci*. 2005;46(1):329–342.
33. Eastlake K, Heywood WE, Banerjee P, et al. Comparative proteomic analysis of normal and gliotic PVR retina and contribution of Müller glia to this profile. *Exp Eye Res*. 2018;177:197–207.
34. Hollborn M, Krausse C, Iandiev I, et al. Glial cell expression of hepatocyte growth factor in vitreoretinal proliferative disease. *Lab Invest*. 2004;84(8):963–972.
35. Percie du Ser N, Hurst V, Ahluwalia A, et al. The ARRIVE guidelines 2.0: updated guidelines for reporting animal research. *BMC Vet Res*. 2020;16:242.
36. Goldaracena MB, Garcia-Layana A, Pastor JC, Saornil MA, De La Fuente F, Gayoso MJ. The role of retinotomy in an experimental rabbit model of proliferative vitreoretinopathy. *Curr Eye Res*. 1997;16(5):422–427.
37. Hida T, Chandler DB, Sheta SM. Classification of the stages of proliferative vitreoretinopathy in a refined experimental model in the rabbit eye. *Graefes Arch Clin Exp Ophthalmol*. 1987;225(4):303–307.
38. Assil KK, Hartzer M, Weinreb RN, Nehorayan M, Ward T, Blumenkranz M. Liposome suppression of proliferative vitreoretinopathy. Rabbit model using antimetabolite encapsulated liposomes. *Invest Ophthalmol Vis Sci*. 1991;32(11):2891–2897.
39. Fastenberg DM, Diddie KR, Dorey K, Ryan SJ. The role of cellular proliferation in an experimental model of massive periretinal proliferation. *Am J Ophthalmol*. 1982;93(5):565–572.

Investigative Ophthalmology & Visual Science

40. Santiago CP, Gimmen MY, Lu Y, et al. Comparative analysis of single-cell and single-nucleus RNA-sequencing in a rabbit model of retinal detachment-related proliferative vitreoretinopathy. *Ophthalmol Sci*. 2023;3(4):100335.
41. Velnar T, Bailey T, Smrkolj V. The wound healing process: an overview of the cellular and molecular mechanisms. *J Int Med Res*. 2009;37(5):1528–1542.
42. Dunn WB, Hardin JH, Spicer SS. Brief report: ultrastructural localization of myeloperoxidase in human neutrophil and rabbit heterophil and eosinophil leukocytes. *Blood*. 1968;32(6):935–944.
43. Baggiolini M, Hirsch JG, De Duve C. Resolution of granules from rabbit heterophil leukocytes into distinct populations by zonal sedimentation. *J Cell Biol*. 1969;40(2):529–541.
44. Horn RG, Spicer SS, Wetzel BK. Phagocytosis of bacteria by heterophil leukocytes: acid and alkaline phosphatase cytochemistry. *Am J Pathol*. 1964;45:327–335.
45. Brown WJ, Shannon WA, Snell WJ. Specific and azurophilic granules from rabbit polymorphonuclear leukocytes. I. Isolation and characterization of membrane and content subfractions. *J Cell Biol*. 1983;96(4):1030–1039.
46. De Schaepdrijver L, Simoens P, Lauwers H, De Geest JP. Retinal vascular patterns in domestic animals. *Res Vet Sci*. 1989;47(1):34–42.
47. Ninomiya H, Inomata T, Kanemaki N. Microvascular architecture of the rabbit eye: a scanning electron microscopic study of vascular corrosion casts. *J Vet Med Sci*. 2008;70(9):887–892.
48. Retinal circulation in man and animals. *Br J Ophthalmol*. 1954;38(7):441.
49. Peiffer R, Pohm-Thorsen L, Corcoran K. Models in Ophthalmology and Vision Research. In: *The Biology of the Laboratory Rabbit*. 2nd ed. Cambridger, MA: Academic Press; 1994:409–433.
50. Zhang Q, Guo Y, Kang M, et al. p21CIP/WAF1 saRNA inhibits proliferative vitreoretinopathy in a rabbit model. *PloS One*. 2023;18(2):e0282063.
51. Reitblat O, Barayev E, Gal-Or O, Tsessler M, Dotan A. Intravitreal tissue plasminogen activator injection for the treatment of proliferative vitreoretinopathy in a rabbit model. *Ophthalmic Res*. Published online June 30, 2022, doi:10.1159/000525745. Online ahead of print.
52. Moon SW, Sun Y, Warther D, et al. New model of proliferative vitreoretinopathy in rabbit for drug delivery and pharmacodynamic studies. *Drug Deliv*. 2018;25(1):600–610.
53. Velez G, Weingarden AR, Lei H, Kazlauskas A, Gao G. SU9518 inhibits proliferative vitreoretinopathy in fibroblast and genetically modified Müller cell–induced rabbit models. *Invest Ophthalmol Vis Sci*. 2013;54(2):1392.
54. Yang S, Li H, Yao H, et al. Long noncoding RNA ERLR mediates epithelial-mesenchymal transition of retinal pigment epithelial cells and promotes experimental proliferative vitreoretinopathy. *Cell Death Differ*. 2021;28(8):2351–2366.
55. Wong CW, Cheung N, Ho C, Barathi V, Storm G, Wong TT. Characterisation of the inflammatory cytokine and growth factor profile in a rabbit model of proliferative vitreoretinopathy. *Sci Rep*. 2019;9(1):15419.
56. Ozer MA, Polat N, Ozen S, Ogurel T, Parlakpinar H, Vardi N. Histopathological and ophthalmoscopic evaluation of apocynin on experimental proliferative vitreoretinopathy in rabbit eyes. *Int Ophthalmol*. 2017;37(3):599–605.
57. Khanum BNMK, Guha R, Sur VP, et al. Pirfenidone inhibits post-traumatic proliferative vitreoretinopathy. *Eye*. 2017;31(9):1317–1328.
58. Zhou Q, Xu G, Zhang X, Cao C, Zhou Z. Proteomics of post-traumatic proliferative vitreoretinopathy in rabbit retina reveals alterations to a variety of functional proteins. *Curr Eye Res*. 2012;37(4):318–326.
59. Pao SI, Lin LT, Chen YH, Chen CL, Chen JT. MicroRNA-4516 suppresses proliferative vitreoretinopathy development via negatively regulating OTX1. *PloS One*. 2022;17(6):e0270526.
60. Datlibagi A, Zein-El-Din A, Frohly M, Willermain F, Delporte C, Motulsky E. Experimental models to study epithelial-mesenchymal transition in proliferative vitreoretinopathy. *Int J Mol Sci*. 2023;24(5):4509.
61. Zahn G, Volk K, Lewis GP, et al. Assessment of the integrin $\alpha5\beta1$ antagonist JSM6427 in proliferative vitreoretinopathy using in vitro assays and a rabbit model of retinal detachment. *Invest Ophthalmol Vis Sci*. 2010;51(2):1028–1035.
62. Jin H, Cai W, Yu D, Fan J, Liu Q, Yu J. Development of proliferative vitreoretinopathy is attenuated by chicken ovalbumin upstream promoter transcriptional factor 1 via inhibiting epithelial-mesenchymal transition. *Discov Med*. 2022;34(172):103–113.
63. Hirose F, Kiryu J, Tabata Y, et al. Experimental proliferative vitreoretinopathy in rabbits by delivery of bioactive proteins with gelatin microspheres. *Eur J Pharm Biopharm*. 2018;129:267–272.
64. Khoroshilova-Maslova IP, Leparskaya NL, Nabieva MM, Andreeva LD. Experimental modeling of proliferative vitreoretinopathy. an experimental morphological study. *Bull Exp Biol Med*. 2015;159(1):100–102.
65. Dong L, Han H, Huang X, et al. Idelalisib inhibits experimental proliferative vitroretinopathy. *Lab Investig J Tech Methods Pathol*. 2022;102(12):1296–1303.
66. Velez G, Weingarden AR, Tucker BA, Lei H, Kazlauskas A, Young MJ. Retinal pigment epithelium and Müller progenitor cell interaction increase Müller Progenitor cell expression of PDGFRα and ability to induce proliferative vitreoretinopathy in a rabbit model. *Stem Cells Int*. 2012;2012:106486.
67. Yao H, Ge T, Zhang Y, et al. BMP7 antagonizes proliferative vitreoretinopathy through retinal pigment epithelial fibrosis in vivo and in vitro. *FASEB J*. 2019;33(3):3212–3224.
68. Sternberg P, Machemer R. Subretinal proliferation. *Am J Ophthalmol*. 1984;98(4):456–462.
69. Trese MT, Chandler DB, Machemer R. Subretinal strands: ultrastructural features. *Graefes Arch Clin Exp Ophthalmol*. 1985;223(1):35–40.
70. Lewis H, Aaberg TM, Abrams GW, McDonald HR, Williams GA, Mieler WF. Subretinal membranes in proliferative vitreoretinopathy. *Ophthalmology*. 1989;96(9):1403–1414; discussion 1414-1415.
71. Mudhar HS. A brief review of the histopathology of proliferative vitreoretinopathy (PVR). *Eye*. 2020;34(2):246–250.
72. Hoerster R, Muether PS, Vierkotten S, Hermann MM, Kirchhof B, Fauser S. Upregulation of TGF-ß1 in experimental proliferative vitreoretinopathy is accompanied by epithelial to mesenchymal transition. *Graefes Arch Clin Exp Ophthalmol*. 2014;252(1):11–16.
73. Wallyn RH, Hilton GF. Subretinal fibrosis in retinal detachment. *Arch Ophthalmol*. 1979;97(11):2128–2129.
74. Machemer R. Surgical approaches to subretinal strands. *Am J Ophthalmol*. 1980;90(1):81–85.
75. Gilbert C, Hiscott P, Unger W, Grierson I, Mcleod D. Inflammation and the formation of epiretinal membranes. *Eye*. 1988;2(S1):S140–S156.
76. Baudouin C, Gordon WC, Baudouin F, et al. Immunohistologic study of epiretinal membranes in proliferative vitreoretinopathy. *Am J Ophthalmol*. 1990;110(6):593–598.
77. Charteris DG, Hiscott P, Grierson I, Lightman SL. Proliferative vitreoretinopathy: lymphocytes in epiretinal membranes. *Ophthalmology*. 1992;99(9):1364–1367.
78. Esser P, Heimann K, Wiedemann P. Macrophages in proliferative vitreoretinopathy and proliferative diabetic retinopathy: differentiation of subpopulations. *Br J Ophthalmol*. 1993;77(11):731–733.

Investigative Ophthalmology & Visual Science

79. Cheng L, Yu H, Yan N, Lai K, Xiang M. Hypoxia-inducible factor-1α target genes contribute to retinal neuroprotection. *Front Cell Neurosci*. 2017;11:20, https://www.frontiersin.org/article/10.3389/fncel.2017.00020.
80. Jung Y, Isaacs JS, Lee S, Trepel J, Liu ZG, Neckers L. Hypoxia-inducible factor induction by tumour necrosis factor in normoxic cells requires receptor-interacting protein-dependent nuclear factor kappa B activation. *Biochem J*. 2003;370(Pt 3):1011–1017.
81. Alves CH, Fernandes R, Santiago AR, Ambrósio AF. Microglia contribution to the regulation of the retinal and choroidal vasculature in age-related macular degeneration. *Cells*. 2020;9(5):1217.
82. Lee SY, Surbeck JW, Drake M, et al. Increased glial fibrillary acid protein and vimentin in vitreous fluid as a biomarker for proliferative vitreoretinopathy. *Invest Ophthalmol Vis Sci*. 2020;61(5):22–22.
83. Yu AK, Forward KI, Morales SA, et al. Co-Expression of RPE65 and GFAP with EMP2 in human proliferative vitreoretinopathy (PVR) membranes. *Invest Ophthalmol Vis Sci*. 2010;51(13):6089–6089.

Investigative Ophthalmology & Visual Science